TEMPERATURE MINIMUM HEATING IN SOLAR FLARES BY RESISTIVE DISSIPATION OF ALFVEN WAVES

by

A. Gordon Emslie and P.A. Sturrock

National Aeronautics and Space Administration
Grant NGL 05-020-272
Grant NAGW-92

Office of Naval Research
Contract N00014-75-C-0673

SUIPR Report No. 856

August 1981

INSTITUTE FOR PLASMA RESEARCH
STANFORD UNIVERSITY, STANFORD, CALIFORNIA

TEMPERATURE MINIMUM HEATING IN SOLAR FLARES BY RESISTIVE DISSIPATION OF ALFVÉN WAVES

A. Gordon Emslie* and P.A. Sturrock**

Institute for Plasma Research, Stanford University

Via Crespi, Stanford, CA 94305, U.S.A.

Abstract. We examine the possibility that the strong heating produced at temperature-minimum levels during solar flares is due to resistive dissipation of Alfvén waves generated by the primary energy release process in the corona. It is shown how, for suitable parameters, these waves can carry their energy essentially undamped into the temperature-minimum layers and can then produce a degree of heating consistent with observations.

*Present Address: Department of Physics, The University of Alabama in Huntsville, Huntsville, AL 35899, U.S.A.

**Also Department of Applied Physics, Stanford University

1. Introduction

There now exists substantial observational evidence for strong heating of the temperature-minimum (T_{min}) region in solar flares (Machado et al., 1978; Cook, 1979; Cook and Brueckner, 1979; Canfield et al., 1980). This observed temperature rise amounts to some 100-200 K, corresponding to a specific energy input of some 10-20 erg $cm^{-3}s^{-1}$ at these levels (Machado et al., 1978). It appears to be difficult to reconcile this amount of heating with a primary flare energy release in the corona and subsequent transport of this energy through the atmosphere by either particles or radiation (Machado et al., 1978; Emslie and Machado, 1979). Emslie and Machado (1979), among others (e.g., Sturrock, 1980), have therefore proposed that the T_{min} region is heated by joule dissipation of currents. They do not consider the generation of these currents, but they do point out that such currents must have a very fine spatial structure ($\lesssim 10^6$ cm) since otherwise the magnetic field associated with them would be unacceptably large.

According to Machado et al. (1978), the total energy dissipated at T_{min} levels during flares is small compared to the total flare energy budget. Thus, in explaining T_{min} heating, the total energy release requirement is not difficult to meet. The problem instead is to find a mechanism for transporting this energy efficiently from the primary release site to the T_{min} level of the atmosphere (or to explain how part of the energy can be released at the T_{min} level).

Emslie and Machado (1979) note that, because of the relatively low temperatures and low fractional ionization level of the plasma at T_{min} levels, the plasma resistivity η there is much larger than at any other point in the solar atmosphere (see Figure 1). Hence the energy carried by electric currents generated in the corona may reach the T_{min} layers of the atmosphere, essentially unattenuated, and then be efficiently damped due to the large resistivity.

The transverse scale of such coronal current patterns generated during flares may well be small enough (see Section 3) to satisfy the constraints imposed by Emslie and Machado (1979).

In this paper we therefore investigate the possibility that electric currents associated with Alfvén-wave perturbations, generated by the primary flare energy release in the corona, are responsible for heating the temperature-minimum region during flares. In Section 2 we discuss the propagation and damping of these waves. In Section 3 we investigate the heating rates effected by this mechanism for a range of model parameters and so place constraints on these parameters if the mechanism is to be effective at T_{min} heating. In Section 4 we discuss the results obtained.

2. Propagation and Damping of Alfvén Waves in the Solar Atmosphere

We wish to analyze the transmission of energy along magnetic field lines from coronal heights down to the temperature-minimum region. In the MHD approximation, there are three modes of propagation: the slow and the fast mangetoacoustic modes, and the Alfvén mode. In a complex situation involving non-uniform plasma and magnetic field, the group velocity of the magnetoacoustic modes must be expected in the course of propagation to depart from the direction of the magnetic field, even if the group velocity is initially directed along the field (Weinberg, 1962). On the other hand, the group velocity of Alfvén waves is always parallel to the magnetic field. Energy in the Alfvén mode will therefore remain in that mode as long as the wavelength is small compared with the length scale for variations of the field and plasma.

The scale height for variation of the plasma properties varies over a wide range in the sun's atmosphere. The wavelength of a propagating Alfvén wave also varies with height since the Alfvén speed varies. We find that, for

waves of interest, the wavelength is much less than the scale height for variation of density (for instance) throughout the corona and in the upper part of the transition region (see Section 3). We begin by considering this region and postpone until later in this section discussion of the lower transition region in which the density varies abruptly.

Since we are concerned only with the propagation of energy along magnetic field lines, we shall ignore the magnetoacoustic modes and consider only the Alfvén mode. We begin by considering a simple model in which the magnetic field is uniform and vertical, but we shall allow for non-zero resisitivity and for variation of density with height. We shall subsequently consider the additional effect of slow variation of the magnetic field strength with height.

The equation of motion of the plasma is

$$\rho \frac{d\underset{\sim}{v}}{dt} = - \underset{\sim}{\nabla} p + \underset{\sim}{j} \times \underset{\sim}{B} \quad , \tag{2.1}$$

where we use modified Gaussian units (Jackson, 1962) for electromagnetic quantities, and we have ignored the gravitational force since we shall be concerned with wave frequencies much higher than the Brunt-Vaisala frequency (Unno et al., 1979). The unperturbed state is characterized by the density $\rho_o(z)$, the pressure $p_o(z)$ and magnetic field strength $\underset{\sim}{B}_o(z) = (0,0,B_o)$. To first order, the perturbation in the equilibrium state of the plasma and field satisfies

$$\rho_o \frac{d\delta\underset{\sim}{v}}{dt} = - \underset{\sim}{\nabla} \delta p + \delta \underset{\sim}{j} \times \underset{\sim}{B}_o \quad . \tag{2.2}$$

On using the Maxwell equations

$$\frac{1}{c} \frac{\partial \underset{\sim}{B}}{\partial t} = - \underset{\sim}{\nabla} \times \underset{\sim}{E} \quad . \tag{2.3}$$

and

$$\nabla \times \underset{\sim}{B} = 4\pi \underset{\sim}{j} \tag{2.4}$$

and the Ohm's law relationship

$$\eta \underset{\sim}{j} = \underset{\sim}{E} + \frac{1}{c} \underset{\sim}{v} \times \underset{\sim}{B} \ , \tag{2.5}$$

where the resistivity η is taken to be a scalar, we obtain

$$\frac{\partial \underset{\sim}{B}}{\partial t} = \nabla \times (\underset{\sim}{v} \times \underset{\sim}{B}) + \frac{c}{4\pi} \eta \nabla^2 \underset{\sim}{B} - \frac{c}{4\pi} \nabla \eta \times (\nabla \times \underset{\sim}{B}) \ . \tag{2.6}$$

On combining equations (2.2), (2.4) and the appropriate perturbed form of (2.6), we obtain the wave equation

$$\frac{\partial^2 \delta \underset{\sim}{B}}{\partial t^2} = \nabla \times \left\{ \left[- \frac{1}{\rho_o} (\nabla \delta p) + \frac{1}{4\pi\rho} (\nabla \times \delta \underset{\sim}{B}) \times \underset{\sim}{B}_o \right] \times \underset{\sim}{B}_o \right\}$$

$$+ \frac{c}{4\pi} \eta \nabla^2 \left(\frac{\partial \delta \underset{\sim}{B}}{\partial t} \right) - \frac{c}{4\pi} \nabla \eta \times \left(\nabla \times \frac{\partial \delta \underset{\sim}{B}}{\partial t} \right) \ . \tag{2.7}$$

Since the Alfvén mode is transverse, we may without loss of generality consider that $\delta \underset{\sim}{B} = (0, \delta B_y, 0)$. Further, since the Alfvén mode involves divergence-free motion, the pressure gradient plays no role. (Our assumption that the wavelength is small compared with the scale height in fact makes it possible to neglect this term not only for the Alfvén mode but also for the fast and slow magnetosonic modes.) Hence we may write

$$\delta B_y = b(z) e^{i(k_x x - \omega t)} \ . \tag{2.8}$$

Equation (2.7) then reduces to

$$-\omega^2 b = \frac{d}{dz}\left(V^2 \frac{db}{dz}\right) - \frac{ic\omega}{4\pi}\frac{d\eta}{dz}\frac{db}{dz} - \frac{ic\eta\omega}{4\pi}\left(-k_x^2 + \frac{d^2}{dz^2}\right) b \quad , \tag{2.9}$$

where V is the Alfvén speed given by

$$V^2 = \frac{B_o^2}{4\pi\rho_o} \quad . \tag{2.10}$$

If ρ_o (hence V) is independent of z and if $\eta = 0$, then b varies as $e^{ik_z z}$, where k_z satisfies the dispersion relation for Alfvén waves:

$$\omega^2 = V^2 k_z^2 \quad . \tag{2.11}$$

Since, for the problem of interest, $\eta \neq 0$, the Alfvén waves will be damped. If V varies slowly with z, then an Alfvén wave will retain its identity but its amplitude will vary in the course of propagation. We may consider both of these effects at the same time by expressing $b(z)$ in the form

$$b(z) = A(z) \exp\left[i\int_0^z k_z(z')dz'\right] \quad . \tag{2.12}$$

We find that, to lowest order in the effects of η and the variation of V, the expression given by (2.12) indeed satisfies the wave equation (2.9) if the amplitude $A(z)$ varies as follows:

$$A(z) = A(0)\left(\frac{V(z)}{V(0)}\right)^{-1/2} \exp\left[-\frac{1}{2}\int_0^z \frac{dz'}{L_D(z')}\right] \quad . \tag{2.13}$$

In deriving this expression, we have assumed that the wave is propagating in the z-direction. The "damping length" L_D is expressible as

$$\frac{1}{L_D} = \frac{1}{L_\perp} + \frac{1}{L_\parallel} \tag{2.14}$$

where $L_\perp$ and $L_\parallel$, the "transverse" and "parallel" damping lengths, are given by the expressions

$$L_\perp = \frac{4\pi V}{c\eta k_x^2} = \frac{4\pi V \ell^2}{c\eta} \tag{2.15}$$

and

$$L_\parallel = \frac{4\pi V^3}{c\eta\omega^2} \quad , \tag{2.16}$$

and we write ℓ for $(k_x)^{-1}$.

If the energy flux being carried by an Alfvén wave is represented by S, and if the actual perturbation in the magnetic field due to the wave is given by the real part of expression (2.12), then

$$S = \frac{1}{8\pi} VA^2 \ . \tag{2.17}$$

Hence, from Equation (2.13),

$$S(z) = S(0) \exp\left[-\int_0^z \frac{dz'}{L_D(z')}\right] \quad . \tag{2.18}$$

This equation will be used to estimate the damping of Alfvén waves in the neighborhood of the temperature-minimum region.

As an Alfvén wave of given frequency propagates down through the corona into the transition region, it encounters a density gradient which is initially small but becomes larger and larger. At some location, the assumption that the wave length is small compared with the characteristic length scale of variation of density becomes invalid. Below that point, the density gradient becomes very steep, so that there is in fact a sharp change in

density in less than one wavelength. In this situation, part of the wave energy will be transmitted and part will be reflected.

The component of the wave vector parallel to the z-axis is given by

$$k_z = \omega V^{-1} = \omega B^{-1} (4\pi m_p n)^{1/2} \quad , \tag{2.19}$$

where n is the number density both of electrons and protons. To a fair approximation, the transition region may be regarded as a region in which the heat flux F (erg $cm^{-2}s^{-1}$) is constant (Athay, 1976). Then, using the Spitzer (1962) conductivity, the characteristic length scale for the temperature change L_T, defined by

$$L_T = T \, (dT/dz)^{-1} \quad , \tag{2.20}$$

is given by

$$L_T = \alpha T^{7/2} \, F^{-1} \quad , \tag{2.21}$$

where $\alpha \approx 10^{-6}$ erg $cm^{-1}s^{-1}K^{-7/2}$. The gas pressure, given by

$$P = 2nkT \quad , \tag{2.22}$$

is approximately constant in the transition region so that the density scale height is equal to the temperature scale height L_T. Hence the critical condition that the density gradient is comparable with the Alfvén wave number may be expressed as

$$k_z L_T = 1 \quad . \tag{2.23}$$

On using Equations (2.19), (2.21) and (2.22), we find that this condition occurs at the "critical" layer where the density and temperature are n_c and T_c, given by

$$n_c = 10^{12.4}\, F^{-1/3}\, P^{7/6}\, B^{-1/3}\, \omega^{1/3} \qquad (2.24)$$

and

$$T_c = 10^{3.2}\, F^{1/3}\, P^{-1/6}\, B^{1/3}\, \omega^{-1/3} \quad . \qquad (2.25)$$

As far as transmission and reflection are concerned, the important quantity is the jump in density in going from this critical region into the chromosphere, which we write as

$$\Theta = \frac{\rho_{ch}}{\rho_c} \approx \frac{n_{ch}}{n_c} = \frac{T_c}{T_{ch}} \quad . \qquad (2.26)$$

We see from Equation (2.25) that this may be expressed as

$$\Theta = 10^{3.2}\, T_{ch}^{-1}\, F^{1/3}\, P^{-1/6}\, B^{1/3}\, \omega^{-1/3} \quad . \qquad (2.27)$$

We write the wave amplitude on the coronal side of the transition region as

$$b_- (z,t) = Ae^{i\left[k_-(z-z_J) - \omega t\right]} + R_B\, Ae^{i\left[-k_-(z-z_J) - \omega t\right]} \qquad (2.28)$$

and the wave amplitude on the chromospheric (transmitted) side as

$$b_+ (z,t) = T_B\, Ae^{i\left[k_+(z-z_J) - \omega t\right]} \quad , \qquad (2.29)$$

where the jump is assumed to occur at $z = z_J$. On noting that b is continuous across the jump and, from Equation (2.9), that

$$V_-^2 \frac{db_-}{dz} = V_+^2 \frac{db_+}{dz} \quad , \qquad (2.30)$$

we find that the reflection and transmission coefficients are given by

$$R_B = \frac{\Theta^{1/2} - 1}{\Theta^{1/2} + 1} \quad , \quad T_B = \frac{2\,\Theta^{1/2}}{\Theta^{1/2} + 1} \quad . \tag{2.31}$$

On noting that the energy flux is proportional to b^2V , we see that the coefficients for the reflection and transmission of energy are given by

$$R_E = \frac{\left(\Theta^{1/2} - 1\right)^2}{\left(\Theta^{1/2} + 1\right)^2} \quad , \quad T_E = \frac{4\Theta^{1/2}}{\left(\Theta^{1/2} + 1\right)^2} \quad . \tag{2.32}$$

If energy is suddenly released at the top of a loop, then a fraction T_E of that energy is transmitted to the chromosphere and photosphere after a time t_1 , where t_1 is the time it takes for an Alfvén wave to propagate from the top of the loop to the base. After an additional time $2t_1$, an additional fraction $R_E T_E$ is transmitted, etc. (We have assumed that the wave is not significantly damped in the corona; this will be verified *a posteriori* in Section 3.) Hence we see that the characteristic decay time τ_D of the energy flow to the lower atmosphere is given by

$$\tau_D = -\frac{2t_1}{\ell n R_E} \quad . \tag{2.33}$$

For example, consider the range of values $\Theta = 10 - 100$. For this range, we find that $R_E = .27 - .67$, so that $\tau_D/t_1 = 1.5 - 5.0$. In a symmetrical configuration, the energy will escape equally through both feet of the loop.

We have so far considered that the magnetic field is uniform and vertical. In a real solar flux tube, neither of these conditions will be satisfied. Weinberg (1962) has discussed very generally the effect upon wave propagation of variations in the parameters entering the wave equation. His analysis confirms that for Alfvén waves, even in a general magnetic-field configuration, energy propagates along magnetic field lines and that the wave amplitude varies according to Equation (2.13).

However, Weinberg's analysis also sheds light on the variation of the wave vector during propagation. If we consider propagation along a field line which is curved but lies in a plane, we find that the components of the wave vector along the field line ($k_{\parallel}$) and normal to the plane (k_n) are unaffected by the curvature, but the rate of change of the component $k_{\perp}$ normal to the field line acquires the following contribution

$$\frac{dk_{\perp}}{ds} = - 2\kappa\, k_{\parallel} \quad , \tag{2.34}$$

where $\kappa(s)$ is the curvature of the field line. In order to assess the influence of this effect, we may consider the case that a wave begins at the top of a loop ($s = 0$) with $k_{\perp} = 0$. Then at the base of the loop, where $s = L$,

$$\frac{k_{\perp}(L)}{k_{\parallel}(L)} = - 2\int_0^L \frac{ds\ \kappa(s)}{\left[V(s)/V(L)\right]} \quad . \tag{2.35}$$

As a result of the rapid increase in density as s approaches L, the dominant contribution to the integral comes from the last (the lowest) density scale height. If, as is likely, the angular deflection $\int\kappa(s)ds$ of a magnetic field line is small in the lowest density scale height, we may neglect the change in the wave vector due to curvature of the field lines.

The wave vector will also be modified during propagation by the convergence or divergence of the field lines. If the convergence is "one-dimensional" in the sense that there is convergence or divergence in one of the transverse directions (x, say) but not in the other direction (y), then k_x scales with the magnetic field strength but k_y is unaffected. If, as another example, the field configuration has cylindrical symmetry, then both of the transverse components of the wave vector scale as $B^{1/2}$. We shall, for definiteness, consider the latter case in the examples to be discussed in the next section.

3. Model Parameters

Table 1

The variation of $b(z)$ with z, as given by Equations (2.13), (2.28) and (2.29), depends not only on the values of the wave parameters ω and $\ell_o (\equiv \ell$ at the top of the loop), but also on the features of the flare loop itself. We have investigated four possible loop models, shown in Table 1. These models differ only in their magnetic field strengths and geometries, with the coronal field strengths in the range 100-300 G and the field strengths near the footpoints of the loop in the range 100-900 G. We consider a narrow flux tube with "cylindrical" symmetry. For the purposes of calculation, a convenient form for the variation of B_o with z is the model considered by Antiochos and Sturrock (1976),

$$\frac{B_o(z)}{B_o(0)} = \sec^2 \left(\frac{z}{L} \arccos \Gamma^{-1/2} \right) , \qquad (3.1)$$

(although this model was derived for a field configuration of somewhat different symmetry). The area factor ("compression ratio") Γ for each model considered is tabulated in Table I. Below $z = L$, the background field strength was taken to be uniform and equal to $B_o(L)$. The chromospheric variations of temperature, density, ionization level and resistivity with height were taken from model 'F1' of Machado et al. (1980) and are shown in Figure 1, plotted against the column number density N (cm^{-2}) as independent variable. The resistivity was assumed classical (Spitzer, 1962), with allowance made for the effect of ion-neutral collisions near the temperature minimum (Emslie and Machado, 1979). The possibility of anomalous resistivity in the region of flare energy release will be considered below.

Figure 1
Figure 2

We solved the relevant equations for each atmospheric model for a range of both $\nu (= \omega/2\pi)$ and ℓ_o, the resulting behavior of the quantity Q (local energy deposition rate per unit volume) is shown in Figure 2. The results in

the figure correspond to an initial perturbation amplitude $b(0) = 1G$; for other values of $b(0)$, the energy deposition rate scales as $[b(0)]^2$. The shaded areas in the figure represent the approximate location of the strong T_{min} temperature enhancements reported by Machado et al. (1978); the maximum of $Q(N)$ must lie in this region if the heating mechanism proposed in the present paper is to be effective. For ℓ_o values much larger than 10^6 cm , the $L_{\parallel}$ term in Equation (2.14) completely dominates [cf. Equations (2.15) and (2.16)], and so the results are similar to those for $\ell_o = 10^6$ cm . Similarly, for $\nu \ll 1$ Hz , the $L_{\perp}$ term dominates, so that results for such low frequencies need not be shown either.

It is immediately obvious from the figure that the proposed mechanism is effective at heating T_{min} layers only if the parameters ν and ℓ_o fall within the ranges

$$\nu \lesssim 10 \text{ Hz} \tag{3.2}$$

and

$$\ell_o \gtrsim 10^5 \text{ cm} \quad . \tag{3.3}$$

Further, only for models with high photospheric magnetic field strengths [resulting in higher Alfvén velocities and so lower damping rates in the chromosphere - see Equations (2.15) and (2.16)] is a satisfactory situation found (e.g. models c, d in the case $\ell_o = 10^5$ cm , $\nu = 1$ Hz) . This result is encouraging, since the results of Tarbell et al. (1979) indicate that such high values of the magnetic field strength at the photosphere are indeed appropriate.

The required values of ν and ℓ_o may be compared with independent estimates of their likely values. Recent analyses of the time structure of flare-associated hard X-ray bursts (Dennis et al., 1981) reveal structures with time-scales of the order of a few tenths of a second, with no significant structure

on time-scales smaller than this. Thus, based on this data, we would expect the highest frequency of any flare-associated disturbance to be of order 10 Hz , in good agreement with the values required (Figure 2). Further, on the basis that magnetic reconnection in an unstable arch is the source of the primary energy release, we should expect ℓ_o to be comparable to the width of a magnetic "island" ℓ_I (Spicer, 1976, 1977). From Spicer's (1976) Equations (4.35) and (4.54) (see also Furth et al., 1963), we find that

$$\ell_I \approx \left(\frac{\rho \eta^2 c^4}{4\pi K^3 B_o^2}\right)^{1/5} , \tag{3.4}$$

where K is the wavenumber of the perturbation inducing the magnetic reconnection. Inserting numerical values and noting that $K \approx L^{-1}$, we obtain, using the coronal model given in Table I,

$$\ell_I \approx 10^{5.5}\left(\frac{\rho L^3}{T^3 B_o^2}\right)^{1/5} \approx 10^{3.3} \text{ cm} \tag{3.5}$$

(see also Van Hoven, 1976). In deriving this value we have used the classical plasma resistivity (Spitzer, 1962). The presence of turbulence in the reconnection region will increase η and so ℓ_I . For instance, ℓ_I is increased to $\approx 10^5$ cm if the turbulent resistivity exceeds the Spitzer resistivity by a factor of about 2×10^4 . Hence the required value $\ell_o \approx 10^5$ cm is not incompatible with the "island thickness" likely to arise during reconnection.

As mentioned in Section 1, the observations and empirical model-fitting of Machado et al. (1978) indicate flare-associated temperature rises of some 100-200 K at T_{min} levels, corresponding [cf. their Equations (18) and (19)] to a specific energy deposition rate of some 10-20 erg $cm^{-3}s^{-1}$, depending on whether the observed structure is "average" or "bright". From the results of Figure 2 (which, we recall, are normalized to unit initial perturbation ampli-

tude $b(0)$) , we therefore deduce that the required value of the magnetic-field fluctuation generated by reconnection should have the value

$$b(0) \gtrsim 5G \tag{3.6}$$

in order for Q to agree with these observationally deduced values. This value of $b(0)$ also corresponds to a total (i.e. depth-integrated) energy deposition rate of some 5×10^{7} erg $cm^{-2}s^{-1}$ in the T_{min} layers (see dashed curves in Figure 2); this is also in good agreement with Machado et al.'s (1978) estimates.

Such a value of $b(0)$ results in a value of b of $\gtrsim 15$ G just below the transition zone [see Equation (2.31)]. The value of b further increases to $\gtrsim 40$ G at a column depth $N \gtrsim 3\times10^{22}$ cm^{-2} , because the increase of ρ and the corresponding decrease of V [Equation (2.10)], leads to an increase of b [Equation (2.13)]. For larger N , b falls off due to resistive damping of the waves which overcomes any increase in b due to the effect of increasing density. These values of b are much smaller than the ambient field strength B_o in the models of interest, as is necessary to justify the linear analysis of Section 2. Finally, we note that, for the values of ν and ℓ_o emerging from our study, the wavelength in the corona is much less than the temperature length scale in that region. Also, both $L_{\parallel}$ and $L_{\perp}$ [Equations (2.15) and (2.16)] are, for classical resistivity, much larger than L , so that the wave damping in the corona ($z < z_J$) is negligible. In fact, even if the resistivity in the region of magnetic reconnection exceeds the Spitzer (1962) value by the factor of $\gtrsim 10^4$ required to reconcile ℓ_o with the thickness of the reconnection region (see above), it is still easily demonstrated that both $L_{\parallel}$ and $L_{\perp}$ are large compared to the size of such a region. We thus see that the modeling assumptions of $\lambda \ll L_T$ and $L_D \gg L$ made in Section 2 are justified.

4. Discussion and Conclusions

As pointed out above (Section 1), the total energy liberated at T_{min} levels during solar flares is a relatively small factor in the total energy budget of a flare, and therefore the constraint that the observed strong heating at T_{min} levels places on a candidate heating mechanism does not hinge upon the total energy supply but simply upon the existence of a mechanism to transport energy throughout the solar atmosphere from the corona until it is efficiently damped at T_{min} levels. The mechanism proposed in the present paper permits virtually undamped propagation of energy through the corona and upper chromosphere, coupled with an efficient damping mechanism at T_{min} levels.

We conclude from the results of the previous section that Alfvén waves of moderate amplitude can, through resistive dissipation of their associated alternating currents, account for the observed temperature enhancements at T_{min} levels during solar flares. However, it is interesting to note that the propagation of energy from the primary release site in the corona to the T_{min} level is relatively slow, with an associated timescale

$$\tau = \int \frac{dz}{V(z)} \quad . \tag{4.1}$$

For the coronal and chromospheric models adopted in this paper (Table I), we can readily compute this integral numerically; we find that (with τ measured in seconds)

$$\tau \simeq \frac{10^4}{B_{o,ph}} \quad , \tag{4.2}$$

where $B_{o,ph}$(gauss) is the strength of the photospheric magnetic field [the exact field geometry in the corona is unimportant, since the disturbance travel time

in the corona represents only a small contribution to τ; see Equation (2.33)]. This is much larger than the time-scale quoted by Emslie et al. (1978) for an MHD disturbance to propagate in the upper chromosphere, because of the much larger densities (and correspondingly low Alfvén velocities) appropriate to the T_{min} region. Nevertheless, for the plausible range of values $B_{o,ph} \gtrsim 300$ G, the timescale is much smaller than the 10 minute delay time between the impulsive phase of the flare and the T_{min} enhancements observed by Machado et al. (1978). This therefore implies that, for the proposed heating model to be valid, magnetic disturbances must be generated in the corona (or elsewhere) long after the impulsive phase of the flare. It is possible that these disturbances can reveal themselves in other observational signatures, such as radio emission; however, it is unlikely that their associated currents will produce observationally detectable effects in locations other than the T_{min} region, because of the very low resistivity in all other parts of the atmosphere.

Finally, we note that Equation (4.2) represents a strong observational test of the present model. If Equation (4.2) is valid, no enhancement at the T_{min} level should be detected until a time measurably later than the impulsive phase of the flare -- as indicated, for example, by the hard X-ray burst. It appears that data do not yet exist against which to check this consequence of the model.

Acknowledgements

We thank John Leach for helpful criticism of an early version of this manuscript. This work was supported by NASA grants NGL 05-020-272 and NAGW-92, and ONR contract N00014-75-C-0673.

References

Antiochos, S.K. and Sturrock, P.A.: 1976, Solar Phys. 49, 359.

Athay, R.G.: 1976, The Solar Chromosphere and Corona: the Quiet Sun, Reidel Dordrecht, p. 314.

Canfield, R.C., Brown, J.C., Brueckner, G.E., Cook, J.W., Craig, I.J.D., Doschek, G.A., Emslie, A.G., Hénoux, J.-C., Lites, B.W., Machado, M.E., and Underwood, J.H.: 1980, in P.A. Sturrock, ed., Solar Flares - A Monograph From Skylab Solar Workshop II, (Boulder: Colorado Associated Press).

Cook, J.W.: 1979, Astrophys. J. 234, 378.

Cook, J.W. and Brueckner, G.E.: 1979, Astrophys. J., 227, 645.

Dennis, B.R., Frost, K.J., and Orwig, L.E.: 1981, Astrophys. J. (Letters), 244, L167.

Emslie, A.G., Brown, J.C., and Donnelly, R.F.: 1978, Solar Phys. 57, 175.

Emslie, A.G. and Machado, M.E.: 1979, Solar Phys. 64, 129.

Furth, H.P., Killeen, J., and Rosenbluth, M.N.: 1963, Phys. Fluids 6, 459.

Jackson, J.D.: 1962, Classical Electrodynamics, Wiley, New York, p. 617.

Lites, B.W. and Cook, J.W.: 1979, Astrophys. J. 228, 598.

Machado, M.E., Avrett, E.H., Vernazza, J.E., and Noyes, R.W.: 1980, Astrophys. J. 242, 336.

Machado, M.E., Emslie, A.G., and Brown, J.C.: 1978, Solar Phys. 58, 363.

Spicer, D.S.: 1976, NRL Report 8036.

Spicer, D.S.: 1977, Solar Phys. 53, 305.

Spitzer, L.W.: 1962, Physics of Fully Ionized Gases, 2nd ed., Interscience, New York.

Tarbell, T.D., Title, A.M., and Schoolman, S.A.: 1979, Astrophys. J. 229, 387.

Unno, W., Osaki, Y., Ando, H., and Shibahashi, H.: 1979, Nonradial Oscillations of Stars, University of Tokyo Press, p. 11.

Weinberg, S.: 1962, Phys. Rev. 126, 1899.

Table I

Flare Loop Models

Model	Loop half-length L (cm)	Coronal Temperature T_c (K)	Coronal Density $n_c(cm^{-3})$	Chromospheric Model Adopted	Field Strength at Loop Apex $B_o(0)$ (G)	Area Factor $\Gamma = \frac{B_{phot}}{B_{apex}}$
a	3×10^9	10^7	3×10^9	F1 (Machado et al., 1980)	100	1
b					100	3
c					300	1
d					300	3

Figure Captions

Figure 1. Chromospheric model adopted (from Machado *et al.*, 1980, model 'F1'). Shown, as a function of column depth N, are x - the ionization fraction, n - the number density, T - the temperature, h - the height above the photosphere ($\tau_{5000} = 1$), and η - the plasma resistivity, assumed classical (see Emslie and Machado, 1979).

Figure 2. Energy deposition rate Q (solid) and depth-integrated deposition rate $\int Q dz$ (dashed) versus N. Each diagram refers to a different set of (ν, ℓ_o) values as shown around the border, while within each diagram the letters a through d refer to the coronal magnetic field geometry of the model (see Table I). The shaded areas correspond to the location of the temperature minimum (cf. Figure 1); Q should peak in this depth interval for the model to be effective at heating T_{min} levels of the atmosphere.

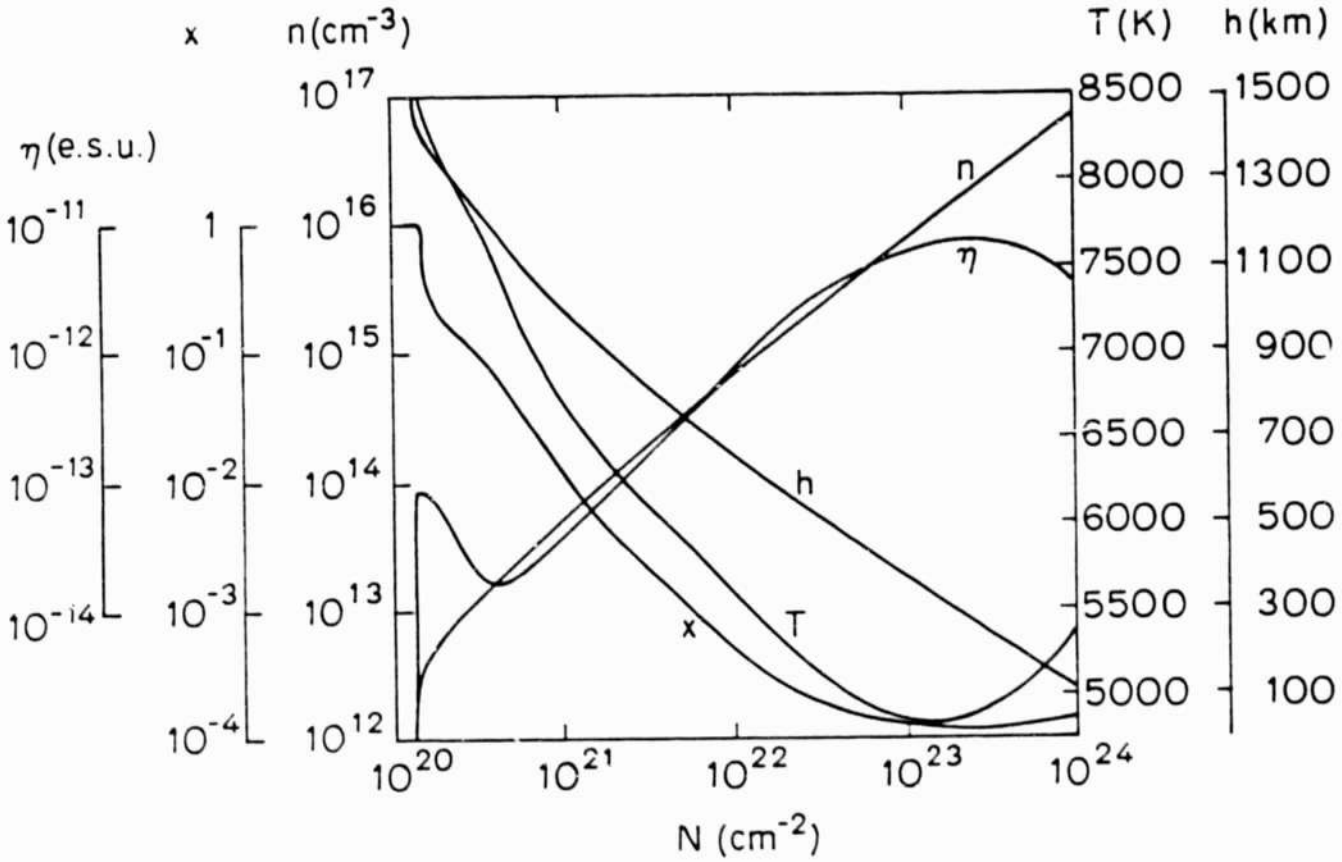
x
n(cm⁻³)
T(K)
h(km)
η(e.s.u.)
10⁻¹¹
10⁻¹²
10⁻¹³
10⁻¹⁴
1
10⁻¹
10⁻²
10⁻³
10⁻⁴
10¹⁷
10¹⁶
10¹⁵
10¹⁴
10¹³
10¹²
8500
8000
7500
7000
6500
6000
5500
5000
1500
1300
1100
900
700
500
300
100
n
η
h
x
T
10²⁰
10²¹
10²²
10²³
10²⁴
N (cm⁻²)

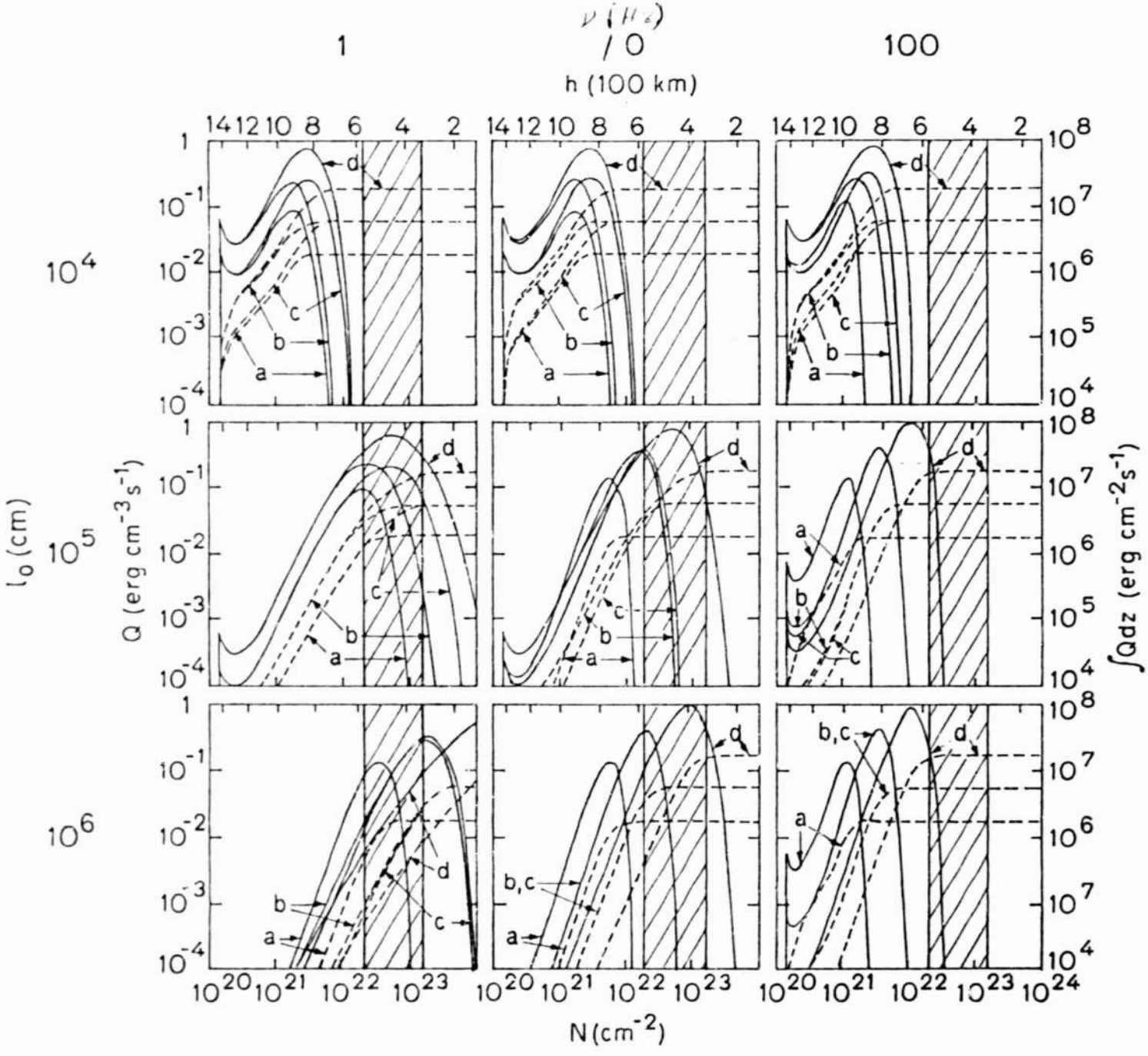
ν (Hz)
1
10
100
h (100 km)
14 12 10 8 6 4 2
l_0 (cm)
10^4
10^5
10^6
Q (erg cm^{-3}s^{-1})
$\int$Qdz (erg cm^{-2}s^{-1})
N(cm^{-2})
10^{20} 10^{21} 10^{22} 10^{23} 10^{24}
a
b
c
d
b,c

Figure 2